



1 Strong Sensitivity of the Isotopic Composition of Methane to the 2 Plausible Range of Tropospheric Chlorine

3

4 Sarah A. Strode^{1,2,*}, James S. Wang^{1,2,**}, Michael Manyin^{2,3}, Bryan Duncan², Ryan Hossaini⁴,
5 Christoph A. Keller^{1,2}, Sylvia E. Michel⁵, James W. C. White⁵

6

7 ¹Universities Space Research Association, Columbia, MD, USA

8 ²NASA Goddard Space Flight Center, Greenbelt, MD, USA

9 ³SSAI, Lanham, MD, USA

10 ⁴Lancaster Environment Centre, Lancaster University, Lancaster, UK

11 ⁵Institute of Arctic and Alpine Research, University of Colorado, Boulder, CO, USA

12 *correspondence to: sarah.a.strode@nasa.gov

13 **Now at the Institute for Advanced Sustainability Studies, Potsdam, Germany

14

15

16 **Abstract.** The ¹³C isotopic ratio of methane, $\delta^{13}\text{C}$ of CH₄, provides additional constraints on the CH₄ budget to
17 complement the constraints from CH₄ observations. The interpretation of $\delta^{13}\text{C}$ observations is complicated, however,
18 by uncertainties in the methane sink. The reaction of CH₄ with Cl is highly fractionating, increasing the relative
19 abundance of ¹³CH₄, but there is currently no consensus on the strength of the tropospheric Cl sink. We use a set of
20 GEOS global model simulations with different predicted Cl fields to test the sensitivity of the $\delta^{13}\text{C}$ of CH₄ to the
21 diversity of Cl output from chemical transport models. We find that $\delta^{13}\text{C}$ is highly sensitive to both the amount and
22 geographic distribution of Cl. Simulations with Cl providing 0.28% or 0.66% of the total CH₄ loss bracket the $\delta^{13}\text{C}$
23 observations for a fixed set of emissions. Thus, even when Cl provides only a small fraction of the total CH₄ loss and
24 has a small impact on total CH₄, it provides a strong lever on $\delta^{13}\text{C}$. The geographic distribution and seasonal cycle of
25 Cl also impacts the hemispheric gradient and seasonal cycle of $\delta^{13}\text{C}$. The large effect of Cl on $\delta^{13}\text{C}$ compared to total
26 CH₄ broadens the range of CH₄ source mixtures that can be reconciled with $\delta^{13}\text{C}$ observations. Stronger constraints
27 on tropospheric Cl are necessary to improve estimates of CH₄ sources from $\delta^{13}\text{C}$ observations.

28

29 1. Introduction

30

31 The global budget of methane is of great interest due to methane's role as a greenhouse gas, ozone precursor,
32 and sink of the hydroxyl radical. Despite extensive study, major uncertainties in the methane budget remain, with
33 top-down and bottom-up estimates often yielding different results (Kirschke et al., 2013; Saunio et al., 2016; Saunio
34 et al., 2017, and refs therein) for the strength of specific source types. Furthermore, the resumed increase of methane
35 concentrations beginning in 2007 (Dlugokencky et al., 2009; Rigby et al., 2008) can be explained by multiple



36 hypotheses including an increase in fossil fuel emissions (Turner et al., 2016;Thompson et al., 2015;Hausmann et al.,
37 2016), an increase in fossil fuel emissions combined with a decrease in biomass burning (Worden et al., 2017), an
38 increase in biogenic sources (Schaefer et al., 2016;Nisbet et al., 2016), or a decrease in hydroxyl concentrations
39 (Turner et al., 2017;Rigby et al., 2017). Variations in hydroxyl concentrations may also be important for the decrease
40 in methane growth from 1999-2006 (McNorton et al., 2016).

41 Observations and modeling of methane's carbon isotopes provides additional information on methane
42 sources since individual sources differ in their ^{13}C to ^{12}C ratio ($\delta^{13}\text{C}$). Isotopic information can be used to better
43 constrain methane sources (e.g. Thompson et al., 2015; Mikaloff Fletcher et al., 2004b, a) and infer how the source
44 mixture changed over glacial (e.g. Hopcroft et al., 2018; Fischer et al., 2008; Bock et al., 2017), millennial (e.g. Ferretti
45 et al., 2005; Houweling et al., 2008), and decadal timescales (e.g. Nisbet et al., 2016; Schaefer et al., 2016; Kai et al.,
46 2011; Schwietzke et al., 2016; Thompson et al., 2018). However, there are considerable uncertainties in the processes
47 that control methane's isotopic composition that may confound source apportionment studies. Many modeling studies
48 use a single value for the isotopic ratio of each source, while in reality sources such as wetlands, biomass burning, and
49 natural gas show large regional or environment-dependent variations in their isotopic signature (Ganesan et al., 2018;
50 Brownlow et al., 2017; Dlugokencky et al., 2011; Schwietzke et al., 2016; Sherwood et al., 2017).

51 The isotopic composition of atmospheric methane is also sensitive to methane's sinks. Reaction with OH,
52 the principal loss for atmospheric methane, has a kinetic isotope effect (KIE) of -5.4‰ ($\alpha=k_{13}/k_{12}=0.9946$) to -3.9‰
53 ($\alpha=0.9961$) (Saueressig et al., 2001; Cantrell et al., 1990) and contributes to the interhemispheric gradient of $\delta^{13}\text{C}$
54 (Quay et al., 1991). Mass balance (Lassey et al., 2007) and observations of the seasonal cycle of $\delta^{13}\text{C}$ versus methane
55 concentration, however, suggest larger apparent KIE values, which may indicate a role for methane oxidation by
56 chlorine (Cl) in the marine boundary layer (MBL) (Allan et al., 2001;Allan et al., 2007) since Cl has a KIE of -61.9‰
57 ($\alpha=0.938$) at 297K (Saueressig et al., 1995). Inclusion of the MBL Cl sink alters the source mixture inferred from
58 inverse modeling of $\delta^{13}\text{CH}_4$ (Rice et al., 2016). Nisbet et al. (2019) point out that interannual variability in the CH_4
59 Cl sink could explain some of the variability of $\delta^{13}\text{C}$. Cl is also an important methane sink in the stratosphere, and the
60 impact of this sink on surface $\delta^{13}\text{C}$ is a source of uncertainty in modeling $\delta^{13}\text{C}$ (Ghosh et al., 2015). Reaction with
61 stratospheric Cl contributes approximately 0.23‰ to the $\delta^{13}\text{C}$ of surface methane and makes a small contribution to
62 the observed trend in surface $\delta^{13}\text{C}$ over the last century (Wang et al., 2002).

63 The global concentration of Cl in the MBL and its role in the methane budget is still uncertain. Cl
64 concentrations are highly variable and not well constrained by direct observations. Modeling work by Hossaini et al.
65 (2016) and Sherwen et al. (2016) suggests that chlorine provides 2-2.5% of tropospheric methane oxidation. This
66 agrees well with estimates based on the isotopic fractionation, which also suggest Cl provides several percent of the
67 total sink (Allan et al., 2007;Platt et al., 2004). However, Gromov et al. (2018) suggest that these are overestimates
68 as values over 1% are inconsistent with the $\delta^{13}\text{C}$ of CO, which is a product of CH_4 oxidation. The recent modeling
69 study of Wang et al. (2019) also suggests a value of 1%. There is thus considerable uncertainty in the role of chlorine
70 in the budget and isotopic composition of methane.

71 Here, we investigate the sensitivity of $\delta^{13}\text{C}$ of CH_4 to tropospheric chlorine concentrations in a global model
72 to better quantify how much uncertainty in the interpretation of $\delta^{13}\text{C}$ is imposed by the uncertainty in Cl. Section 2



73 describes the modeling framework. We present results for total CH₄ and its isotopic composition compared to surface
74 observations in Section 3, and discuss the implications for the global CH₄ budget in Section 4.

75 2. Methods

76

77 2.1 Model Description

78

79 We simulate atmospheric methane with the Goddard Earth Observing System (GEOS) global earth system model
80 (Molod et al., 2015; Nielsen et al., 2017). The model has 72 vertical levels extending from the surface to 1 Pa. We
81 conduct simulations at C90 resolution on the cubed sphere, which corresponds to approximately 100 km horizontal
82 resolution. The simulations' meteorology is constrained to the MERRA-2 reanalysis (Gelaro et al., 2017) using a
83 “replay” method (Orbe et al., 2017). The GEOS replay agrees well with the tropospheric mean age of the GMI CTM
84 (Orbe et al., 2017), which shows reasonable agreement with the age derived from SF₆ observations, albeit with an old
85 bias in the southern hemisphere (Waugh et al., 2013). We thus expect the simulated interhemispheric transport time
86 to be reasonable.

87 The GEOS CH₄ simulation can be interactively coupled to CO and OH (Elshorbany et al., 2016), or run
88 independently with prescribed OH fields. We take the latter approach in this study, since this approach is able to
89 capture many of the observed variations in atmospheric methane (Elshorbany et al., 2016). We prescribe the OH field
90 following (Spivakovsky et al., 2000), but modify the OH to be approximately 20% higher in the Northern Hemisphere
91 than the Southern Hemisphere, consistent with the OH field produced by many global atmospheric chemistry models
92 (Naik et al., 2013; Strode et al., 2015). We also include stratospheric losses for CH₄ from reaction with OH, Cl, and
93 O¹D. These fields are prescribed from output of the Global Modeling Initiative (GMI) chemical transport model
94 (<https://gmi.gsfc.nasa.gov>) (Strahan et al., 2007; Duncan et al., 2007).

95 We implement the CH₄ isotopes in GEOS by separately simulating ¹³CH₄ and ¹²CH₄ tracers. We then calculate
96 total CH₄ as the sum of the two carbon isotopologues and calculate δ¹³C of CH₄ in per mil using the standard definition:

$$97 \quad \delta^{13}\text{C-CH}_4 (\text{‰}) = \left(\frac{[^{13}\text{CH}_4]}{[^{12}\text{CH}_4]} / R_{\text{std}} - 1 \right) * 1000 \quad (1)$$

98 where R_{std}=0.112372 is the peedee belemnite isotopic standard (Craig, 1957). The reaction rates for CH₄+OH,
99 CH₄+Cl, and CH₄+O¹D differ between the ¹²CH₄ and ¹³CH₄ simulations to account for the kinetic isotope effect (KIE).
100 In particular, we assume α values of 0.987 and 0.938 for CH₄+O¹D and CH₄+Cl, respectively (Saueressig et al.,
101 1995; Saueressig et al., 2001). Our standard simulation uses α_{OH} = 0.9946 (Cantrell et al., 1990).

102 Methane from different sources is tracked individually using a “tagged tracer” approach, which allows us to
103 simulate the spatial footprint of CH₄ and δ¹³C-CH₄ from individual sources. We partition each emission source into
104 ¹²CH₄ and ¹³CH₄ emissions according to a source-specific δ¹³C value from the literature, provided in Table 1. The
105 soil sink is applied to each tracer as a fraction of its source, modified to account for faster loss of ¹²CH₄ to soil compared
106 to ¹³CH₄ (α_{soil} = 0.978). Figure 1 shows the CH₄ and δ¹³C-CH₄ footprints of the biomass burning, wetland, and coal
107 + other geologic CH₄ sources from the tagged tracers to illustrate the tagged tracer approach. We note that the δ¹³C
108 values of the surface methane from each source is heavier (less negative) than the emission value for that source (Table



109 1), especially in regions far from the source, because of the fractionating effects of the sinks. Supplemental Fig. S1
110 shows the corresponding footprints for January.

111 2.2 Description of Simulations

112 We simulate the period from 1990 through 2004, and focus our analysis on 2004. We choose 2004 as our endpoint
113 because it lies within the period when methane concentrations remained relatively flat, simplifying our analysis.
114 Ending the simulations in 2004 also avoids much of the uncertainty about the causes of the resumed growth rate in
115 recent years. The isotopic ratios of methane take longer to adjust to a perturbation than total methane (Tans, 1997).
116 Since we wish to begin our simulations with a state that is as close as possible to “spun up”, we choose the initial
117 condition for each tagged tracer based on its present-day distribution and proportion of the total CH₄ and scale it back
118 to 1990 levels such that the total CH₄ is consistent with the global mean CH₄ from surface observations for 1990. We
119 then iteratively adjusted the ¹²C- to ¹³C-CH₄ tracer ratios at the beginning of 1990 to yield a good match to global
120 mean $\delta^{13}\text{C-CH}_4$ observations for 1998, when more $\delta^{13}\text{C-CH}_4$ observations are available. The same initial condition is
121 used for the standard and sensitivity simulations.
122

123 We use interannually-varying emissions of CH₄ from anthropogenic, biomass burning, and wetland sources.
124 Emissions from anthropogenic sources such as oil and gas, energy production, industrial activities, and livestock come
125 from the EDGAR version 4.2 inventory (European Commission, 2011). Biomass burning emissions come from the
126 MACCity inventory (Granier et al., 2011). We treat forest fires as C3 burning and savannas as C4 burning for
127 partitioning the biomass burning emissions between isotopologues. Wetland and rice emissions come from the
128 Vegetation Integrative Simulator for Trace gases (VISIT) terrestrial ecosystem model (Ito and Inatomi, 2012), scaled
129 by 0.69 and 0.895, respectively, for consistency with the Transcom-CH₄ study (Patra et al., 2011). Ocean (Houweling
130 et al., 1999), termite (Fung et al., 1991), and mud volcano emissions (Etiope and Milkov, 2004) are also from the
131 Transcom study (Patra et al., 2011) and have a seasonal cycle but no interannual variability. Initial tests with these
132 emissions showed a substantial underestimate of the CH₄ growth rate. Consequently, we scale up all the emissions
133 by 10% for 1990-1998, and by 6.8% for 1998-2004. We find the resulting emissions lead to a good simulation of the
134 timeseries of surface CH₄ observations from the NOAA GMD (Dlugokencky et al., 2018), especially towards the end
135 of the period (Fig. 2).

136 Our standard simulation (SimStd) uses Cl from the GMI CTM for the tropospheric as well as stratospheric loss
137 of CH₄ by reaction with Cl. Tropospheric Cl concentrations are small in GMI since it does not include very short-
138 lived species, and reaction with Cl represents only 0.28% of the total tropospheric CH₄ loss. We also conduct several
139 sensitivity simulations in which we alter the tropospheric Cl fields (Table 2). Sensitivity simulation SimGC uses Cl
140 from the GEOS-Chem chemistry module within GEOS (Long et al., 2015; Hu et al., 2018). GEOS-Chem v11-02f
141 with fully coupled tropospheric and stratospheric chemistry was used for this simulation, with halogen chemistry as
142 described in Sherwen et al. (2016). SimGC has higher values of tropospheric Cl than SimStd (Figs. 3,4) and leads to
143 0.66% of the total CH₄ loss occurring via Cl. Both SimStd and SimGC are thus below the 1% loss via Cl suggested
144 by (Gromov et al., 2018). We conduct a third sensitivity simulation, SimTom, which uses Cl from the TOMCAT
145 model simulations that include chlorine sources from chlorocarbons (including very short-lived substances), HCl from
146 industry and biomass burning, and very short lived substances (Hossaini et al., 2016). This simulation leads to Cl



147 accounting for 2.5% of CH₄ loss. Finally, we conduct a fourth sensitivity simulation, SimMBL, which modifies the
148 Cl over the oceans at altitudes below 900 hPa (Fig. 3d) to reflect the marine boundary layer distribution suggested by
149 (Allan et al., 2007). This Cl field is described by the following equation:

$$150 \quad \text{Cl_MBL} = 18 \cdot 10^3 \text{ atoms/cm}^3 * (1 + \tanh(3\lambda) * \sin(2\pi * (t-90)/365)) \quad (2)$$

151 where λ is latitude in radians and t is the day of the year. Elsewhere SimMBL uses the Cl field from SimStd. This
152 simulation has the highest percent of CH₄ loss occurring via Cl: 3.9%.

153 We designed the sensitivity experiments to alter the isotopic composition of CH₄ without greatly affecting
154 the total CH₄. Consequently, we reduce the OH concentrations in the SimTom and SimMBL simulations by 2% and
155 4%, respectively, relative to the SimStd OH to offset the effect of increasing Cl. In addition, the SimTom and SimMBL
156 simulations use $\alpha_{\text{OH}}=0.9961$ (Saueressig et al., 2001) rather than $\alpha_{\text{OH}}=0.9946$ (Cantrell et al., 1990) to avoid too much
157 fractionation from the combined Cl and OH sinks. We conduct an additional sensitivity simulation, SimOHp, that
158 uses the same Cl field as SimStd but does not alter the hemispheric ratio of OH. Table 2 summarizes the standard and
159 sensitivity simulations.

160 The four Cl distributions differ in their vertical and horizontal spatial distributions as well as their
161 tropospheric mean (Figs. 3 and 4). The SimStd Cl is largest in the tropics, nearly symmetric between hemispheres,
162 and increases with altitude. Both SimGC and SimTom have Cl that is larger in the Northern Hemisphere than the
163 Southern Hemisphere in the annual mean and reaches a minimum in the mid-troposphere. However, the maximum in
164 lower tropospheric Cl occurs in the tropics in SimGC but in the extratropics in SimTom. This mid-latitude Cl
165 maximum arises because SimTom has high Cl values over east Asia, whereas SimGC Cl is highest over ocean regions
166 (Fig. 4). SimMBL has a strong maximum in the MBL compared to the free troposphere and land regions. Its annual
167 mean Cl concentrations are higher in the Southern Hemisphere (Fig. 3) due to the larger ocean area in the Southern
168 Hemisphere. However, SimMBL includes a strong seasonal shift in peak Cl between the hemispheres.

169 **2.3 Observations**

170 We use surface observations from the NOAA GMD Carbon Cycle Cooperative Global Air Sampling Network to
171 evaluate our simulations. We use the monthly mean observations of total CH₄ (Dlugokencky et al, 2018) and $\delta^{13}\text{C}$ of
172 CH₄ (White et al., 2018) to compare to the monthly mean simulation results. The isotopic measurements were made
173 at the Institute of Arctic and Alpine Research at the University of Colorado and are referenced to the VPDB scale
174 (Zhang and Li, 1990). The analytical uncertainty of the isotopic measurements is 0.06‰. The variability between
175 measurements taken in a given month may, however, be larger, so we use the maximum of analytical uncertainty and
176 the within-month standard deviation as the uncertainty in the monthly mean.
177

178 **3. Results and Discussion**

179 **3.1 Evaluation of Simulated CH₄**

180 We find good agreement between the SimStd simulation and the GMD observations for CH₄ (Fig. 5) for 2004.
181 The latitudinal distribution is well-reproduced, and the simulation captures the elevated concentrations of CH₄
182 observed over Europe in January as well as the January versus July differences in concentration. Overall, the spatial
183
184



185 correlation between SimStd and the observations is 0.93 in January and 0.85 in July. The sensitivity simulations
186 described in Table 2 have little effect on the CH₄ distribution, as shown by the overlapping symbols in Fig. 5c,d.

187

188 3.2 Sensitivity of $\delta^{13}\text{C}$ to Cl

189

190 We next examine the distribution of $\delta^{13}\text{C}$ in SimStd compared to observations. Fig. 6a,b shows both meridional
191 and zonal variability in $\delta^{13}\text{C}$. Background values are less negative (heavier) in the Southern versus Northern
192 Hemisphere (NH) (Fig. 7), a feature seen more strongly in the observations, but there is also variability due to the
193 different source signatures. Areas of biomass burning, such as Tropical Africa, show up as particularly heavy, while
194 regions with large wetland and rice emissions, such as SE Asia, are particularly light. Another prominent feature is
195 the isotopically heavy region in northern Asia in January, which we attribute to the influence of the geologic (including
196 oil, gas, and coal) source in this region (Supp. Fig. S1). This signal is less evident in July, when greater influence
197 from boreal wetlands lightens the isotopic mix. The spatial correlation (r^2) between the SimStd and observed $\delta^{13}\text{C}$ is
198 0.61 in January and 0.75 in July.

199 The sensitivity simulations with altered oxidant concentrations alter the global values of $\delta^{13}\text{C}$, but the geographic
200 patterns remain similar to that of SimStd. The larger Cl sink in SimGC leads to an overall less negative $\delta^{13}\text{C}$, which
201 agrees better than SimStd with observations at Southern Hemisphere (SH) sites but worse in the NH (Figs. 6c,d and
202 7). The isotopic effect of the larger Cl sink in SimTom is compensated by the lower OH and α_{OH} values used in that
203 simulation, flattening the interhemispheric gradient (Figs. 6e,f and 7). In contrast, the very large MBL Cl
204 concentrations in SimMBL lead to an overestimate (insufficiently negative) of the observed $\delta^{13}\text{C}$ (Fig. g,h), but
205 strengthens the interhemispheric gradient. We note that since all simulations began with the same initial conditions
206 but have different sinks, the isotopic composition is not in steady state in 2004 and the results of the sensitivity
207 simulations diverge further with additional years of simulation, with SimMBL becoming clearly inconsistent with
208 observations. We note that while these results highlight the differences in $\delta^{13}\text{C}$ imposed by changing Cl, the absolute
209 values of $\delta^{13}\text{C}$, and hence their agreement with observations, would be different for CH₄ source mixtures with a
210 different average $\delta^{13}\text{C}$.

211 Figure 7 reveals an underestimate in the interhemispheric gradient of $\delta^{13}\text{C}$ in both SimStd and the sensitivity runs
212 compared to the GMD observations. Table 3 presents the observed and simulated $\delta^{13}\text{C}$ interhemispheric gradients
213 calculated as the difference between the $\delta^{13}\text{C}$ values averaged over all sites south of 30°S and the average over sites
214 north of 30°N. SimStd and SimGC show similar underestimates of the observed gradient, and the underestimate is
215 more severe in SimTom. The gradient is improved in SimMBL in January. The differences between simulations
216 reflect differences in the locations where CH₄ oxidation occurs. Fig. 8 shows that the higher Cl values over the NH,
217 particularly China, in SimTom versus SimStd leads to more CH₄ loss occurring in the NH and higher (heavier) $\delta^{13}\text{C}$
218 in the NH. This effect is particularly pronounced over China and Europe. Less fractionation by the OH sink in
219 SimTom leads to lighter values in the SH. Conversely, SimMBL has more loss occurring over the SH oceans in
220 January, leading to heavier $\delta^{13}\text{C}$ in the SH (Fig. 9). This effect is not present in July, when the SimMBL Cl loss shifts



221 to the NH (Fig. S2). The reduced hemispheric difference in OH in SimOHp leads to a small improvement in the
222 hemispheric gradient in $\delta^{13}\text{C}$.

223 We further examine the seasonal cycle of $\delta^{13}\text{C}$ in Fig. 10. We focus on the seasonal cycle at the South Pole
224 Observatory (SPO) site because it is far from large CH_4 sources and thus the seasonal cycle depends strongly on the
225 seasonality of the CH_4 sinks. While all simulations lie mostly within the error bars of the observations, SimMBL has
226 the largest seasonal cycle amplitude, overestimating the seasonal cycle at of the SPO observations with a $\delta^{13}\text{C}$ value
227 that is both too heavy in Feb.-June and too light in Aug.-Nov. In contrast, SimStd and the other sensitivity simulations
228 underestimate the magnitude of the observed seasonal cycle at SPO. Supplemental Fig. S3 shows a large enhancement
229 in the seasonal cycle amplitude between SimMBL and the other simulations for the Cape Grim site in Tasmania
230 (CGO), but only a small change at other sites. This suggests that while MBL Cl is attractive as an explanation for the
231 SH seasonality of $\delta^{13}\text{C}$, this explanation may be inconsistent with the inclusion of non-marine Cl sources.

232

233 3.3 Sensitivity of $\delta^{13}\text{C}$ to the Isotopic Distribution of Sources

234

235 Other factors in addition to the Cl distribution likely contribute to the mismatch between the observed and
236 simulated interhemispheric gradients. Fig. 6 shows the impact of the geologic source on the $\delta^{13}\text{C}$ values over northern
237 Asia. A bias in either the strength or the isotopic composition of this source will impact the interhemispheric gradient.
238 Another likely contributing factor is our use of a globally uniform isotopic ratio for each source type. Ganesan et al.
239 (2018) developed a global map of the isotopic signatures of wetland emissions. We conduct a sensitivity study,
240 SimWet, that parallels SimStd but uses these spatially varying isotopic ratios for the wetland emissions. SimWet
241 increases the amplitude of the seasonal cycle in $\delta^{13}\text{C}$ - CH_4 particularly for northern latitudes sites such as ALT, BRW,
242 and MHD (Supplemental Fig. S3). It has little effect on the seasonal cycle at the SH CGO and SPO sites, where
243 SimMBL shows a large effect on the cycle. SimWet results in improved agreement with the observed interhemispheric
244 gradient (Figs. 6,7; Table 3). Including spatially-varying isotopic signature for other sources as well could further
245 modify the simulated interhemispheric gradient, potentially correcting some of the flat gradient of e.g. the SimTom
246 simulation.

247

248 4. Conclusions

249

250 The role of Cl as a methane sink is a significant uncertainty in the global CH_4 budget, particularly with respect to
251 isotopes. The global distribution of Cl is not well known from observations, and the Cl distributions simulated by
252 global models varies widely from model to model. We investigated the sensitivity of the surface $\delta^{13}\text{C}$ distribution of
253 CH_4 using a series of sensitivity studies with a global 3D model. Given the uncertainties in CH_4 sources and their
254 isotopic ratios, it is not possible to conclude from this study which Cl field is best. However, the differences between
255 the simulations provides insight on the strong lever that tropospheric Cl exerts on the $\delta^{13}\text{C}$ distribution.

256 Our standard and sensitivity simulations all reproduce well the geographic distribution of and temporal evolution
257 of CH_4 observed at the GMD surface sites. However, imposing Cl distributions from a range of chemical transport



258 models used in the scientific community leads to large differences in the simulated distribution of the $\delta^{13}\text{C}$ of CH_4 .
259 The CH_4 sinks from Cl in our SimStd and SimGC simulations are both below 1% of the total CH_4 sink, as suggested
260 by Gromov et al. (2018). Yet the SimStd and SimGC simulations underestimate and overestimate, respectively, the
261 observed $\delta^{13}\text{C}$ in 2004, despite the fact that both include only a relatively small CH_4 sink from Cl.

262 Our ability to reproduce the observed latitudinal distribution of $\delta^{13}\text{C}$ depends not only on the assumed value of
263 global mean Cl, but also its geographic distribution. The detailed halogen chemistry model (TOMCAT) of Hossaini
264 et al. (2016) places the maximum Cl values in the continental NH, in contrast to the large MBL Cl sink used in Allan
265 et al. (2007) to explain SH observations. We find that the NH Cl maximum acts to flatten the interhemispheric gradient
266 of $\delta^{13}\text{C}$, while the MBL Cl sink increases the hemispheric differences in NH winter and also strengthens the seasonal
267 cycle. However, the interhemispheric gradient is also influenced by spatial variation in the isotopic signatures of the
268 sources, complicating this issue.

269 Two values for the fractionating effect of OH (α_{OH}) on $\delta^{13}\text{C}$ (Cantrell et al., 1990; Saueressig et al., 2001) are
270 widely cited in the literature. Combining the TOMCAT Cl fields with the α_{OH} of Saueressig et al. (2001) leads to an
271 underestimate of observed $\delta^{13}\text{C}$, but combining it with the Cantrell et al. (1990) α_{OH} would lead to an overestimate.
272 Reducing uncertainty in the fractionating effect of OH would thus improve our ability to constrain the role of Cl.

273 Observations of the $\delta^{13}\text{C}$ of CH_4 provide an important tool for constraining the CH_4 budget. We find that the
274 range of Cl fields available from current global models leads to a wide range of simulated $\delta^{13}\text{C}$ values. The choice of
275 Cl field thus strongly impacts what CH_4 source mixture best fits $\delta^{13}\text{C}$ observations. Better quantification of the role
276 of Cl in the methane budget is therefore critical for interpreting the $\delta^{13}\text{C}$ observations to their fullest potential.

277

278 **Data Availability**

279 The methane and $\delta^{13}\text{CH}_4$ observations are available from the NOAA GMD website:
280 <https://www.esrl.noaa.gov/gmd/dv/data/>. Output from the GEOS model is on the NASA Center for Climate
281 Simulation (NCCS) system.

282

283 **Author Contributions**

284 SS designed and conducted simulation, performed analysis, and prepared the manuscript. JSW contributed to model
285 development and experiment design. MM contributed to model development. BD contributed to model development
286 and conceptualization. RH and CK contributed inputs to the simulations. SM and JWCW contributed data and aided
287 in its interpretation. All authors contributed to the editing and revising of the manuscript.

288

289 The authors declare no competing interests.

290

291 **Acknowledgements**

292 Computational resources were provided by the NASA Center for Climate Simulation (NCCS). The authors thank
293 Prabir Patra for useful discussions.

294



295 **References**

- 296 Allan, W., Manning, M. R., Lassey, K. R., Lowe, D. C., and Gomez, A. J.: Modeling the variation of $\delta^{13}\text{C}$ in
297 atmospheric methane: Phase ellipses and the kinetic isotope effect, *Global Biogeochemical Cycles*, 15, 467-481,
298 doi:10.1029/2000GB001282, 2001.
- 299 Allan, W., Struthers, H., and Lowe, D.: Methane carbon isotope effects caused by atomic chlorine in the marine
300 boundary layer: Global model results compared with Southern Hemisphere measurements, *Journal of Geophysical*
301 *Research: Atmospheres*, 112, 2007.
- 302 Bock, M., Schmitt, J., Beck, J., Seth, B., Chappellaz, J., and Fischer, H.: Glacial/interglacial wetland, biomass
303 burning, and geologic methane emissions constrained by dual stable isotopic CH_4 ice core records, *Proceedings of*
304 *the National Academy of Sciences*, 114, E5778-E5786, 10.1073/pnas.1613883114, 2017.
- 305 Brownlow, R., Lowry, D., Fisher, R., France, J., Lanoisellé, M., White, B., Wooster, M., Zhang, T., and Nisbet, E.:
306 Isotopic ratios of tropical methane emissions by atmospheric measurement, *Global Biogeochemical Cycles*, 31,
307 1408-1419, 2017.
- 308 Cantrell, C. A., Shetter, R. E., McDaniel, A. H., Calvert, J. G., Davidson, J. A., Lowe, D. C., Tyler, S. C., Cicerone,
309 R. J., and Greenberg, J. P.: Carbon kinetic isotope effect in the oxidation of methane by the hydroxyl radical, *Journal*
310 *of Geophysical Research: Atmospheres*, 95, 22455-22462, 1990.
- 311 Craig, H.: Isotopic Standards for Carbon and Oxygen and Correction Factors for Mass-Spectrometric Analysis OF
312 Carbon Dioxide, *Geochimica Et Cosmochimica Acta*, 12, 133-149, 10.1016/0016-7037(57)90024-8, 1957.
- 313 Dlugokencky, E., Bruhwiler, L., White, J., Emmons, L., Novelli, P., Montzka, S., Masarie, K., Lang, P., Crotwell,
314 A., Miller, J., and Gatti, L.: Observational constraints on recent increases in the atmospheric CH_4 burden,
315 *Geophysical Research Letters*, 36, 10.1029/2009GL039780, 2009.
- 316 Dlugokencky, E., Nisbet, E., Fisher, R., and Lowry, D.: Global atmospheric methane: budget, changes and dangers,
317 *Philosophical Transactions of the Royal Society a-Mathematical Physical and Engineering Sciences*, 369, 2058-
318 2072, 10.1098/rsta.2010.0341, 2011.
- 319 Dlugokencky, E.J., P.M. Lang, A.M. Crotwell, J.W. Mund, M.J. Crotwell, and K.W. Thoning, Atmospheric
320 Methane Dry Air Mole Fractions from the NOAA ESRL Carbon Cycle Cooperative Global Air Sampling Network,
321 1983-2017, Version: 2018-08-01, Path: ftp://afpt.cmdl.noaa.gov/data/trace_gases/ch4/flask/surface/, 2018.
- 322 Duncan, B. N., Strahan, S. E., Yoshida, Y., Steenrod, S. D., and Livesey, N.: Model study of the cross-tropopause
323 transport of biomass burning pollution, *Atmospheric Chemistry and Physics*, 7, 3713-3736, 2007.
- 324 Elshorbany, Y. F., Duncan, B. N., Strode, S. A., Wang, J. S., and Kouatchou, J.: The description and validation of
325 the computationally Efficient $\text{CH}_4\text{-CO-OH}$ (ECCOHv1.01) chemistry module for 3-D model applications,
326 *Geoscientific Model Development*, 9, 799-822, 10.5194/gmd-9-799-2016, 2016.
- 327 Etiope, G., and Milkov, A.: A new estimate of global methane flux from onshore and shallow submarine mud
328 volcanoes to the atmosphere, *Environmental Geology*, 46, 997-1002, 10.1007/s00254-004-1085-1, 2004.
- 329 European Commission, Joint Research Center (JRC)/Netherlands Environmental Assessment Agency (PBL).
330 Emission Database for Global Atmospheric Research (EDGAR), <http://edgar.jrc.ec.europa.eu>.



- 331 Ferretti, D. F., Miller, J. B., White, J. W. C., Etheridge, D. M., Lassey, K. R., Lowe, D. C., Meure, C. M. M., Dreier,
332 M. F., Trudinger, C. M., van Ommen, T. D., and Langenfelds, R. L.: Unexpected Changes to the Global Methane
333 Budget over the Past 2000 Years, *Science*, 309, 1714-1717, 10.1126/science.1115193, 2005.
- 334 Fischer, H., Behrens, M., Bock, M., Richter, U., Schmitt, J., Louergue, L., Chappellaz, J., Spahni, R., Blunier, T.,
335 Leuenberger, M., and Stocker, T. F.: Changing boreal methane sources and constant biomass burning during the last
336 termination, *Nature*, 452, 864, 10.1038/nature06825
337 <https://www.nature.com/articles/nature06825#supplementary-information>, 2008.
- 338 Fung, I., John, J., Lerner, J., Matthews, E., Prather, M., Steele, L., and Fraser, P.: 3-Dimensional Model Synthesis of
339 the Global Methane Cycle, *Journal of Geophysical Research-Atmospheres*, 96, 13033-13065, 10.1029/91JD01247,
340 1991.
- 341 Ganesan, A., Stell, A., Gedney, N., Comyn-Platt, E., Hayman, G., Rigby, M., Poulter, B., and Hornibrook, E.:
342 Spatially Resolved Isotopic Source Signatures of Wetland Methane Emissions, *Geophysical Research Letters*, 45,
343 3737-3745, 2018.
- 344 Gelaro, R., McCarty, W., Suarez, M., Todling, R., Molod, A., Takacs, L., Randles, C., Darmenov, A., Bosilovich,
345 M., Reichle, R., Wargan, K., Coy, L., Cullather, R., Draper, C., Akella, S., Buchard, V., Conaty, A., da Silva, A.,
346 Gu, W., Kim, G., Koster, R., Lucchesi, R., Merkova, D., Nielsen, J., Partyka, G., Pawson, S., Putman, W.,
347 Rienecker, M., Schubert, S., Sienkiewicz, M., and Zhao, B.: The Modern-Era Retrospective Analysis for Research
348 and Applications, Version 2 (MERRA-2), *Journal of Climate*, 30, 5419-5454, 10.1175/JCLI-D-16-0758.1, 2017.
- 349 Ghosh, A., Patra, P., Ishijima, K., Umezawa, T., Ito, A., Etheridge, D., Sugawara, S., Kawamura, K., Miller, J., and
350 Dlugokencky, E.: Variations in global methane sources and sinks during 1910–2010, *Atmospheric Chemistry and*
351 *Physics*, 15, 2595-2612, 2015.
- 352 Granier, C., Bessagnet, B., Bond, T., D'Angiola, A., van der Gon, H. D., Frost, G. J., Heil, A., Kaiser, J. W., Kinne,
353 S., Klimont, Z., Kloster, S., Lamarque, J. F., Liousse, C., Masui, T., Meleux, F., Mieville, A., Ohara, T., Raut, J. C.,
354 Riahi, K., Schultz, M. G., Smith, S. J., Thompson, A., van Aardenne, J., van der Werf, G. R., and van Vuuren, D. P.:
355 Evolution of anthropogenic and biomass burning emissions of air pollutants at global and regional scales during the
356 1980-2010 period, *Climatic Change*, 109, 163-190, 10.1007/s10584-011-0154-1, 2011.
- 357 Gromov, S., Brenninkmeijer, C. A., and Jöckel, P.: A very limited role of tropospheric chlorine as a sink of the
358 greenhouse gas methane, *Atmospheric Chemistry and Physics*, 18, 9831-9843, 2018.
- 359 Hausmann, P., Sussmann, R., and Smale, D.: Contribution of oil and natural gas production to renewed increase in
360 atmospheric methane (2007–2014): top–down estimate from ethane and methane column observations, *Atmospheric*
361 *Chemistry and Physics*, 16, 3227-3244, 2016.
- 362 Hopercoft, P. O., Valdes, P. J., and Kaplan, J. O.: Bayesian Analysis of the Glacial-Interglacial Methane Increase
363 Constrained by Stable Isotopes and Earth System Modeling, *Geophysical Research Letters*, 45, 3653-3663,
364 doi:10.1002/2018GL077382, 2018.
- 365 Hossaini, R., Chipperfield, M. P., Saiz-Lopez, A., Fernandez, R., Monks, S., Feng, W., Brauer, P., and von Glasow,
366 R.: A global model of tropospheric chlorine chemistry: Organic versus inorganic sources and impact on methane
367 oxidation, *Journal of Geophysical Research: Atmospheres*, 121, 14,271-214,297, doi:10.1002/2016JD025756, 2016.



- 368 Houweling, S., Kaminski, T., Dentener, F., Lelieveld, J., and Heimann, M.: Inverse modeling of methane sources
369 and sinks using the adjoint of a global transport model, *Journal of Geophysical Research-Atmospheres*, 104, 26137-
370 26160, 10.1029/1999JD900428, 1999.
- 371 Houweling, S., Dentener, F., and Lelieveld, J.: Simulation of preindustrial atmospheric methane to constrain the
372 global source strength of natural wetlands, *Journal of Geophysical Research-Atmospheres*, 105, 17243-17255,
373 10.1029/2000JD900193, 2000.
- 374 Houweling, S., Van der Werf, G., Goldewijk, K. K., Röckmann, T., and Aben, I.: Early anthropogenic CH₄
375 emissions and the variation of CH₄ and 13CH₄ over the last millennium, *Global Biogeochemical Cycles*, 22, 2008.
- 376 Hu, L., Keller, C., Long, M., Sherwen, T., Auer, B., Da Silva, A., Nielsen, J., Pawson, S., Thompson, M., Trayanov,
377 A., Travis, K., Grange, S., Evans, M., and Jacob, D.: Global simulation of tropospheric chemistry at 12.5 km
378 resolution: performance and evaluation of the GEOS-Chem chemical module (v10-1) within the NASA GEOS Earth
379 system model (GEOS-5 ESM), *Geoscientific Model Development*, 11, 4603-4620, 10.5194/gmd-11-4603-2018,
380 2018.
- 381 Ito, A., and Inatomi, M.: Use of a process-based model for assessing the methane budgets of global terrestrial
382 ecosystems and evaluation of uncertainty, *Biogeosciences*, 9, 759-773, 10.5194/bg-9-759-2012, 2012.
- 383 Kai, F., Tyler, S., Randerson, J., and Blake, D.: Reduced methane growth rate explained by decreased Northern
384 Hemisphere microbial sources, *Nature*, 476, 194-197, 10.1038/nature10259, 2011.
- 385 Kirschke, S., Bousquet, P., Ciais, P., Saunoy, M., Canadell, J. G., Dlugokencky, E. J., Bergamaschi, P., Bergmann,
386 D., Blake, D. R., Bruhwiler, L., Cameron-Smith, P., Castaldi, S., Chevallier, F., Feng, L., Fraser, A., Heimann, M.,
387 Hodson, E. L., Houweling, S., Josse, B., Fraser, P. J., Krummel, P. B., Lamarque, J.-F., Langenfelds, R. L., Le
388 Quere, C., Naik, V., O'Doherty, S., Palmer, P. I., Pison, I., Plummer, D., Poulter, B., Prinn, R. G., Rigby, M.,
389 Ringeval, B., Santini, M., Schmidt, M., Shindell, D. T., Simpson, I. J., Spahni, R., Steele, L. P., Strode, S. A., Sudo,
390 K., Szopa, S., van der Werf, G. R., Voulgarakis, A., van Weele, M., Weiss, R. F., Williams, J. E., and Zeng, G.:
391 Three decades of global methane sources and sinks, *Nature Geoscience*, 6, 813-823, 10.1038/NGEO1955, 2013.
- 392 Lassey, K. R., Etheridge, D. M., Lowe, D. C., Smith, A. M., and Ferretti, D. F.: Centennial evolution of the
393 atmospheric methane budget: what do the carbon isotopes tell us?, *Atmos. Chem. Phys.*, 7, 2119-2139, 10.5194/acp-
394 7-2119-2007, 2007.
- 395 Long, M., Yantosca, R., Nielsen, J., Keller, C., da Silva, A., Sulprizio, M., Pawson, S., and Jacob, D.: Development
396 of a grid-independent GEOS-Chem chemical transport model (v9-02) as an atmospheric chemistry module for Earth
397 system models, *Geoscientific Model Development*, 8, 595-602, 10.5194/gmd-8-595-2015, 2015.
- 398 McNorton, J., Chipperfield, M., Gloor, M., Wilson, C., Feng, W., Hayman, G., Rigby, M., Krummel, P., O'Doherty,
399 S., Prinn, R., Weiss, R., Young, D., Dlugokencky, E., and Montzka, S.: Role of OH variability in the stalling of the
400 global atmospheric CH₄ growth rate from 1999 to 2006, *Atmospheric Chemistry and Physics*, 16, 7943-7956,
401 10.5194/acp-16-7943-2016, 2016.
- 402 Mikaloff Fletcher, S. E., Tans, P. P., Bruhwiler, L. M., Miller, J. B., and Heimann, M.: CH₄ sources estimated from
403 atmospheric observations of CH₄ and its 13C/12C isotopic ratios: 2. Inverse modeling of CH₄ fluxes from
404 geographical regions, *Global Biogeochemical Cycles*, 18, doi:10.1029/2004GB002224, 2004a.



- 405 Mikaloff Fletcher, S. E., Tans, P. P., Bruhwiler, L. M., Miller, J. B., and Heimann, M.: CH₄ sources estimated from
406 atmospheric observations of CH₄ and its ¹³C/¹²C isotopic ratios: 1. Inverse modeling of source processes, *Global*
407 *Biogeochemical Cycles*, 18, doi:10.1029/2004GB002223, 2004b.
- 408 Molod, A., Takacs, L., Suarez, M., and Bacmeister, J.: Development of the GEOS-5 atmospheric general circulation
409 model: evolution from MERRA to MERRA2, *Geoscientific Model Development*, 8, 1339-1356, 10.5194/gmd-8-
410 1339-2015, 2015.
- 411 Monteil, G., Houweling, S., Dlugokenky, E., Maenhout, G., Vaughn, B., White, J., and Rockmann, T.: Interpreting
412 methane variations in the past two decades using measurements of CH₄ mixing ratio and isotopic composition,
413 *Atmospheric chemistry and physics*, 11, 9141-9153, 2011.
- 414 Naik, V., Voulgarakis, A., Fiore, A. M., Horowitz, L. W., Lamarque, J. F., Lin, M., Prather, M. J., Young, P. J.,
415 Bergmann, D., Cameron-Smith, P. J., Cionni, I., Collins, W. J., Dalsoren, S. B., Doherty, R., Eyring, V., Faluvegi,
416 G., Folberth, G. A., Josse, B., Lee, Y. H., MacKenzie, I. A., Nagashima, T., van Noije, T. P. C., Plummer, D. A.,
417 Righi, M., Rumbold, S. T., Skeie, R., Shindell, D. T., Stevenson, D. S., Strode, S., Sudo, K., Szopa, S., and Zeng,
418 G.: Preindustrial to present-day changes in tropospheric hydroxyl radical and methane lifetime from the
419 Atmospheric Chemistry and Climate Model Intercomparison Project (ACCMIP), *Atmospheric Chemistry and*
420 *Physics*, 13, 5277-5298, 10.5194/acp-13-5277-2013, 2013.
- 421 Nielsen, J., Pawson, S., Molod, A., Auer, B., da Silva, A., Douglass, A., Duncan, B., Liang, Q., Manyin, M., Oman,
422 L., Putman, W., Strahan, S., and Wargan, K.: Chemical Mechanisms and Their Applications in the Goddard Earth
423 Observing System (GEOS) Earth System Model, *Journal of Advances in Modeling Earth Systems*, 9, 3019-3044,
424 10.1002/2017MS001011, 2017.
- 425 Nisbet, E., Dlugokenky, E., Manning, M., Lowry, D., Fisher, R., France, J., Michel, S., Miller, J., White, J., and
426 Vaughn, B.: Rising atmospheric methane: 2007–2014 growth and isotopic shift, *Global Biogeochemical Cycles*, 30,
427 1356-1370, 2016.
- 428 Nisbet, E., Manning, M., Dlugokenky, E., Fisher, R., Lowry, D., Michel, S., Myhre, C., Platt, M., Allen, G.,
429 Bousquet, P., Brownlow, R., Cain, M., France, J., Hermansen, O., Hossaini, R., Jones, A., Levin, I., Manning, A.,
430 Myhre, G., Pyle, J., Vaughn, B., Warwick, N., and White, J.: Very Strong. Atmospheric Methane Growth in the 4
431 Years 2014-2017: Implications for the paris Agreement, *Global Biogeochemical Cycles*, 33, 318-342,
432 10.1029/2018GB006009, 2019.
- 433 Orbe, C., Oman, L., Strahan, S., Waugh, D., Pawson, S., Takacs, L., and Molod, A.: Large-Scale Atmospheric
434 Transport in GEOS Replay Simulations, *Journal of Advances in Modeling Earth Systems*, 9, 2545-2560,
435 10.1002/2017MS001053, 2017.
- 436 Patra, P., Houweling, S., Krol, M., Bousquet, P., Belikov, D., Bergmann, D., Bian, H., Cameron-Smith, P.,
437 Chipperfield, M., Corbin, K., Fortems-Cheiney, A., Fraser, A., Gloor, E., Hess, P., Ito, A., Kawa, S., Law, R., Loh,
438 Z., Maksyutov, S., Meng, L., Palmer, P., Prinn, R., Rigby, M., Saito, R., and Wilson, C.: TransCom model
439 simulations of CH₄ and related species: linking transport, surface flux and chemical loss with CH₄ variability in the
440 troposphere and lower stratosphere, *Atmospheric Chemistry and Physics*, 11, 12813-12837, 10.5194/acp-11-12813-
441 2011, 2011.



- 442 Platt, U., Allan, W., and Lowe, D.: Hemispheric average Cl atom concentration from $^{13}\text{C}/^{12}\text{C}$ ratios in atmospheric
443 methane, *Atmos. Chem. Phys.*, 4, 2393-2399, 10.5194/acp-4-2393-2004, 2004.
- 444 Quay, P., King, S., Stutsman, J., Wilbur, D., Steele, L., Fung, I., Gammon, R., Brown, T., Farwell, G., Grootes, P.,
445 and Schmidt, F.: Carbon Isotopic Composition of Atmospheric CH₄: Fossil and Biomass Burning Source Strengths,
446 *Global Biogeochemical Cycles*, 5, 25-47, 10.1029/91GB00003, 1991.
- 447 Rice, A. L., Butenhoff, C. L., Teama, D. G., Röger, F. H., Khalil, M. A. K., and Rasmussen, R. A.: Atmospheric
448 methane isotopic record favors fossil sources flat in 1980s and 1990s with recent increase, *Proceedings of the*
449 *National Academy of Sciences*, 113, 10791-10796, 2016.
- 450 Rigby, M., Prinn, R. G., Fraser, P. J., Simmonds, P. G., Langenfelds, R. L., Huang, J., Cunnold, D. M., Steele, L. P.,
451 Krummel, P. B., Weiss, R. F., O'Doherty, S., Salameh, P. K., Wang, H. J., Harth, C. M., Mühle, J., and Porter, L.
452 W.: Renewed growth of atmospheric methane, *Geophysical Research Letters*, 35, doi:10.1029/2008GL036037,
453 2008.
- 454 Rigby, M., Montzka, S. A., Prinn, R. G., White, J. W., Young, D., O'Doherty, S., Lunt, M. F., Ganesan, A. L.,
455 Manning, A. J., and Simmonds, P. G.: Role of atmospheric oxidation in recent methane growth, *Proceedings of the*
456 *National Academy of Sciences*, 114, 5373-5377, 2017.
- 457 Rotman, D., Tannahill, J., Kinnison, D., Connell, P., Bergmann, D., Proctor, D., Rodriguez, J., Lin, S., Rood, R.,
458 Prather, M., Rasch, P., Considine, D., Ramarosan, R., and Kawa, S.: Global Modeling Initiative assessment model:
459 Model description, integration, and testing of the transport shell, *Journal of Geophysical Research-Atmospheres*,
460 106, 1669-1691, 10.1029/2000JD900463, 2001.
- 461 Saueressig, G., Bergamaschi, P., Crowley, J., Fischer, H., and Harris, G.: Carbon Kinetic Isotope Effect in the
462 Reaction of CH₄ with Cl Atoms, *Geophysical Research Letters*, 22, 1225-1228, 10.1029/95GL00881, 1995.
- 463 Saueressig, G., Crowley, J. N., Bergamaschi, P., Brühl, C., Brenninkmeijer, C. A. M., and Fischer, H.: Carbon 13
464 and D kinetic isotope effects in the reactions of CH₄ with O(1 D) and OH: New laboratory measurements and their
465 implications for the isotopic composition of stratospheric methane, *Journal of Geophysical Research: Atmospheres*,
466 106, 23127-23138, doi:10.1029/2000JD000120, 2001.
- 467 Saunio, M., Bousquet, P., Poulter, B., Peregon, A., Ciais, P., Canadell, J. G., Dlugokencky, E. J., Etiope, G.,
468 Bastviken, D., and Houweling, S.: The global methane budget 2000–2012, *Earth System Science Data (Online)*, 8,
469 2016.
- 470 Saunio, M., Bousquet, P., Poulter, B., Peregon, A., Ciais, P., Canadell, J., Dlugokencky, E., Etiope, G., Bastviken,
471 D., Houweling, S., Janssens-Maenhout, G., Tubiello, F., Castaldi, S., Jackson, R., Alexe, M., Arora, V., Beerling,
472 D., Bergamaschi, P., Blake, D., Brailsford, G., Bruhwiler, L., Crevoisier, C., Crill, P., Covey, K., Frankenberg, C.,
473 Gedney, N., Hoglund-Isaksson, L., Ishizawa, M., Ito, A., Joos, F., Kim, H., Kleinen, T., Krummel, P., Lamarque, J.,
474 Langenfelds, R., Locatelli, R., Machida, T., Maksyutov, S., Melton, J., Morino, I., Naik, V., O'Doherty, S.,
475 Parmentier, F., Patra, P., Peng, C., Peng, S., Peters, G., Pison, I., Prinn, R., Ramonet, M., Riley, W., Saito, M.,
476 Santini, M., Schroeder, R., Simpson, I., Spahni, R., Takizawa, A., Thornton, B., Tian, H., Tohjima, Y., Viovy, N.,
477 Voulgarakis, A., Weiss, R., Wilton, D., Wiltshire, A., Worthy, D., Wunch, D., Xu, X., Yoshida, Y., Zhang, B.,



- 478 Zhang, Z., and Zhu, Q.: Variability and quasi-decadal changes in the methane budget over the period 2000-2012,
479 Atmospheric Chemistry and Physics, 17, 11135-11161, 10.5194/acp-17-11135-2017, 2017.
- 480 Schaefer, H., Fletcher, S. E. M., Veidt, C., Lassey, K. R., Brailsford, G. W., Bromley, T. M., Dlugokencky, E. J.,
481 Michel, S. E., Miller, J. B., Levin, I., Lowe, D. C., Martin, R. J., Vaughn, B. H., and White, J. W. C.: A 21st-century
482 shift from fossil-fuel to biogenic methane emissions indicated by 13CH₄, Science, 352, 80-84,
483 10.1126/science.aad2705, 2016.
- 484 Schwietzke, S., Sherwood, O., Ruhwiler, L., Miller, J., Etiope, G., Dlugokencky, E., Michel, S., Arling, V., Vaughn,
485 B., White, J., and Tans, P.: Upward revision of global fossil fuel methane emissions based on isotope database,
486 Nature, 538, 88-91, 10.1038/nature19797, 2016.
- 487 Sherwen, T., Schmidt, J. A., Evans, M. J., Carpenter, L. J., Großmann, K., Eastham, S. D., Jacob, D. J., Dix, B.,
488 Koenig, T. K., Sinreich, R., Ortega, I., Volkamer, R., Saiz-Lopez, A., Prados-Roman, C., Mahajan, A. S., and
489 Ordóñez, C.: Global impacts of tropospheric halogens (Cl, Br, I) on oxidants and composition in GEOS-Chem,
490 Atmos. Chem. Phys., 16, 12239-12271, 10.5194/acp-16-12239-2016, 2016.
- 491 Sherwood, O., Schwietzke, S., Arling, V., and Etiope, G.: Global Inventory of Gas Geochemistry Data from Fossil
492 Fuel, Microbial and Burning Sources, version 2017, Earth System Science Data, 9, 639-656, 10.5194/essd-9-639-
493 2017, 2017.
- 494 Spivakovsky, C. M., Logan, J. A., Montzka, S. A., Balkanski, Y. J., Foreman-Fowler, M., Jones, D. B. A.,
495 Horowitz, L. W., Fusco, A. C., Brenninkmeijer, C. A. M., Prather, M. J., Wofsy, S. C., and McElroy, M. B.: Three-
496 dimensional climatological distribution of tropospheric OH: Update and evaluation, Journal of Geophysical
497 Research-Atmospheres, 105, 8931-8980, 10.1029/1999jd901006, 2000.
- 498 Strahan, S. E., Duncan, B. N., and Hoor, P.: Observationally derived transport diagnostics for the lowermost
499 stratosphere and their application to the GMI chemistry and transport model, Atmospheric Chemistry and Physics, 7,
500 2435-2445, 2007.
- 501 Strahan, S. E., Douglass, A. R., and Newman, P. A.: The contributions of chemistry and transport to low arctic
502 ozone in March 2011 derived from Aura MLS observations, Journal of Geophysical Research: Atmospheres, 118,
503 1563-1576, 2013.
- 504 Strode, S., Duncan, B., Yegorova, E., Kouatchou, J., Ziemke, J., and Douglass, A.: Implications of carbon monoxide
505 bias for methane lifetime and atmospheric composition in chemistry climate models, Atmospheric Chemistry and
506 Physics, 15, 11789-11805, 2015.
- 507 Tans, P.: A note on isotopic ratios and the global atmospheric methane budget, Global Biogeochemical Cycles, 11,
508 77-81, 10.1029/96GB03940, 1997.
- 509 Thompson, R., Nisbet, E., Pisso, I., Stohl, A., Blake, D., Dlugokencky, E., Helmig, D., and White, J.: Variability in
510 Atmospheric Methane From Fossil Fuel and Microbial Sources Over the Last Three Decades, Geophysical Research
511 Letters, 45, 11499-11508, 10.1029/2018GL078127, 2018.
- 512 Thompson, R. L., Stohl, A., Zhou, L. X., Dlugokencky, E., Fukuyama, Y., Tohjima, Y., Kim, S. Y., Lee, H., Nisbet,
513 E. G., and Fisher, R. E.: Methane emissions in East Asia for 2000–2011 estimated using an atmospheric Bayesian
514 inversion, Journal of Geophysical Research: Atmospheres, 120, 4352-4369, 2015.



515 Turner, A., Jacob, D., Benmergui, J., Wofsy, S., Maasackers, J., Butz, A., Hasekamp, O., and Biraud, S.: A large
516 increase in US methane emissions over the past decade inferred from satellite data and surface observations,
517 Geophysical Research Letters, 43, 2218-2224, 10.1002/2016GL067987, 2016.

518 Turner, A. J., Frankenberg, C., Wennberg, P. O., and Jacob, D. J.: Ambiguity in the causes for decadal trends in
519 atmospheric methane and hydroxyl, Proceedings of the National Academy of Sciences, 114, 5367-5372, 2017.

520 Wang, J. S., McElroy, M. B., Spivakovsky, C. M., and Jones, D. B. A.: On the contribution of anthropogenic Cl to
521 the increase in $\delta^{13}\text{C}$ of atmospheric methane, Global Biogeochemical Cycles, 16, 20-21-20-11, 2002.

522 Wang, X., Jacob, D., Eastham, S., Sulprizio, M., Zhu, L., Chen, Q., Alexander, B., Sherwen, T., Evans, M., Lee, B.,
523 Haskins, J., Lopez-Hilfiker, F., Thornton, J., Huey, G., and Liao, H.: The role of chlorine in global tropospheric
524 chemistry, Atmospheric Chemistry and Physics, 19, 3981-4003, 10.5194/acp-19-3981-2019, 2019.

525 Waugh, D., Crotwell, A., Dlugokencky, E., Dutton, G., Elkins, J., Hall, B., Hints, E., Hurst, D., Montzka, S.,
526 Mondeel, D., Moore, F., Nance, J., Ray, E., Steenrod, S., Strahan, S., and Sweeney, C.: Tropospheric SF₆: Age of
527 air from the Northern Hemisphere midlatitude surface, Journal of Geophysical Research-Atmospheres, 118, 11429-
528 11441, 10.1002/jgrd.50848, 2013.

529 White, J.W.C., B.H. Vaughn, and S.E. Michel, University of Colorado, Institute of Arctic and Alpine Research
530 (INSTAAR), Stable Isotopic Composition of Atmospheric Methane (^{13}C) from the NOAA ESRL Carbon Cycle
531 Cooperative Global Air Sampling Network, 1998-2017, Version: 2018-09-24, Path:
532 ftp://aftp.cmdl.noaa.gov/data/trace_gases/ch4c13/flask/, 2018.

533 Worden, J. R., Bloom, A. A., Pandey, S., Jiang, Z., Worden, H. M., Walker, T. W., Houweling, S., and Röckmann,
534 T.: Reduced biomass burning emissions reconcile conflicting estimates of the post-2006 atmospheric methane
535 budget, Nature communications, 8, 2227, 2017.

536 Zhang, Q.-L. and Li, W.-J.: A Calibrated Measurement of the Atomic Weight of Carbon, Chinese Science Bulletin
537 35, 290, doi: 10.1360/sb1990-35-4-290, 1990.

538
539



540 **Table 1:** Emission source references and $\delta^{13}\text{C}$ values

Source	Reference	IAV	$\delta^{13}\text{C}$ (‰) ^a	CH ₄ Source (Tg yr ⁻¹) ^b
Animals (enteric fermentation)	EDGAR	Y	-62	102
C3 Biomass Burning (Forests)	MACCity	Y	-26	16
C4 Biomass Burning (Savannas)	MACCity	Y	-15	10
Coal, energy, and industry	EDGAR	Y	-35	6
Geologic (oil/gas/non-coal fuels, volcanos)	EDGAR, Transcom	Y, except volcanos	-40	124
Waste (solid and animal waste, wastewater)	EDGAR	Y	-55	74
Ocean	Transcom	N	-59	8
Rice	Visit model	Y	-63	44
Termites	Transcom	N	-57	22
Wetlands	Visit model	Y	-60	149

541 ^a $\delta^{13}\text{C}$ values from Dlugokencky et al., 2011; Lassey et al., 2007; Monteil et al., 2011; Houweling et al., 2000 and refs
 542 therein

543 ^bValues for 2004

544 **Table 2:** Oxidants for the Standard and sensitivity simulations

Simulation	[CI] _{Trop} ^a (molec cm ⁻³)	CI Model ^b	CI Reference	OH modification ^c
SimStd	210	GMI	(Strahan et al., 2007; Rotman et al., 2001; Strahan et al., 2013; Duncan et al., 2007)	$\alpha = 0.9946$
SimGC	384	GEOSChem	(Sherwen et al., 2016)	$\alpha = 0.9946$
SimTom	1710	TOMCAT	(Hossaini et al., 2016)	-2% [OH] $\alpha = 0.9961$
SimOHp	210	GMI	See SimStd	Not modified for 20% higher in NH
SimMBL	2810	Tanh function below 900hPa over ocean; GMI elsewhere	(Allan et al., 2007)	-4% [OH] $\alpha = 0.9961$

546 ^aConcentration of CI averaged over the troposphere

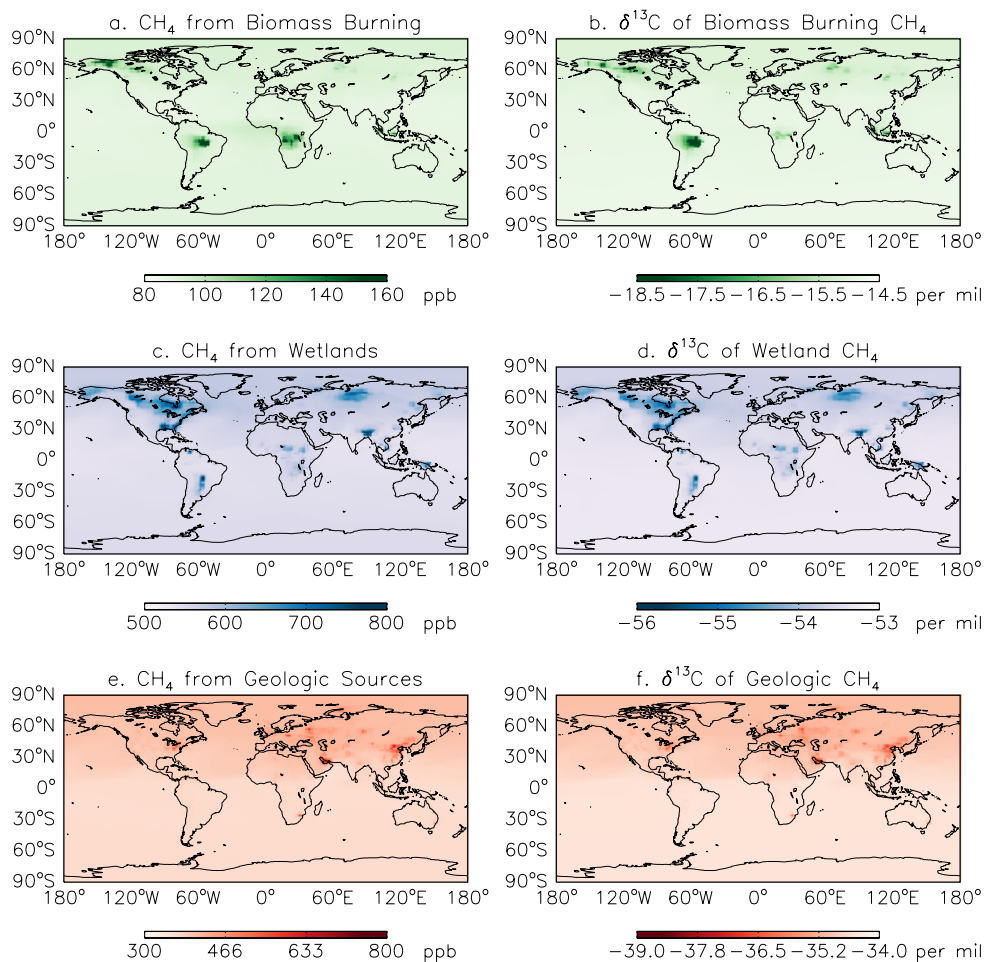
547 ^bName of the model that generated the offline CI field

548 ^cChanges to [OH] or α_{OH} compared to SimStd

549 **Table 3:** Observed and Simulated Interhemispheric Gradient in $\delta^{13}\text{C}$ -CH₄

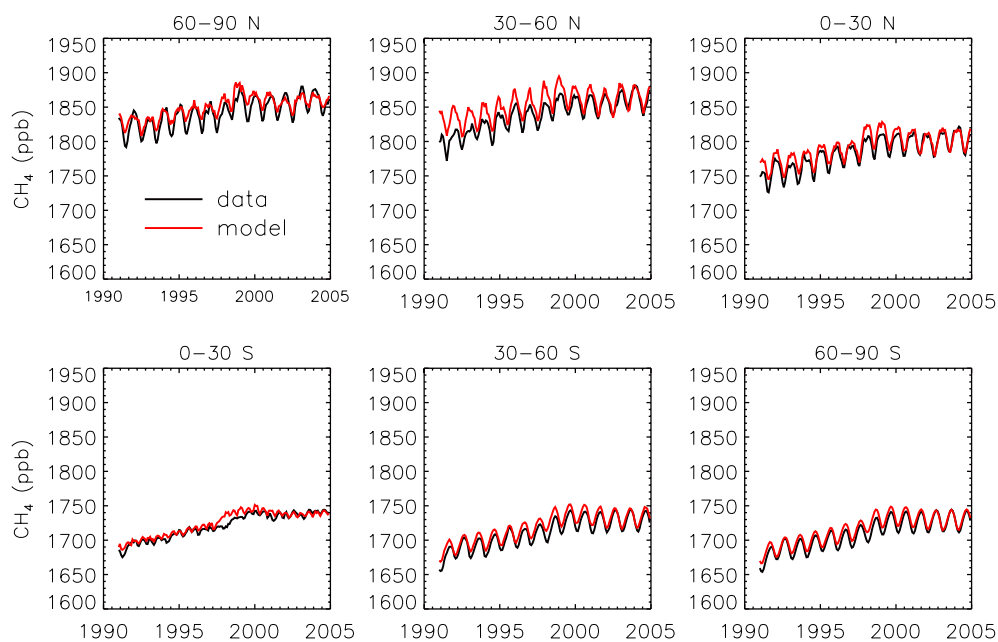
	Jan. Gradient (‰) ^a	July Gradient (‰) ^a
GMD Obs	0.36	0.28
SimStd	0.17	0.11
SimGC	0.17	0.098
SimTom	0.051	0.010
SimMBL	0.30	0.13
SimOHp	0.22	0.15
SimWet	0.28	0.25

551 ^aAverage $\delta^{13}\text{C}$ -CH₄ at GMD site locations south of 30°S minus average $\delta^{13}\text{C}$ -CH₄ at locations north of 30°N



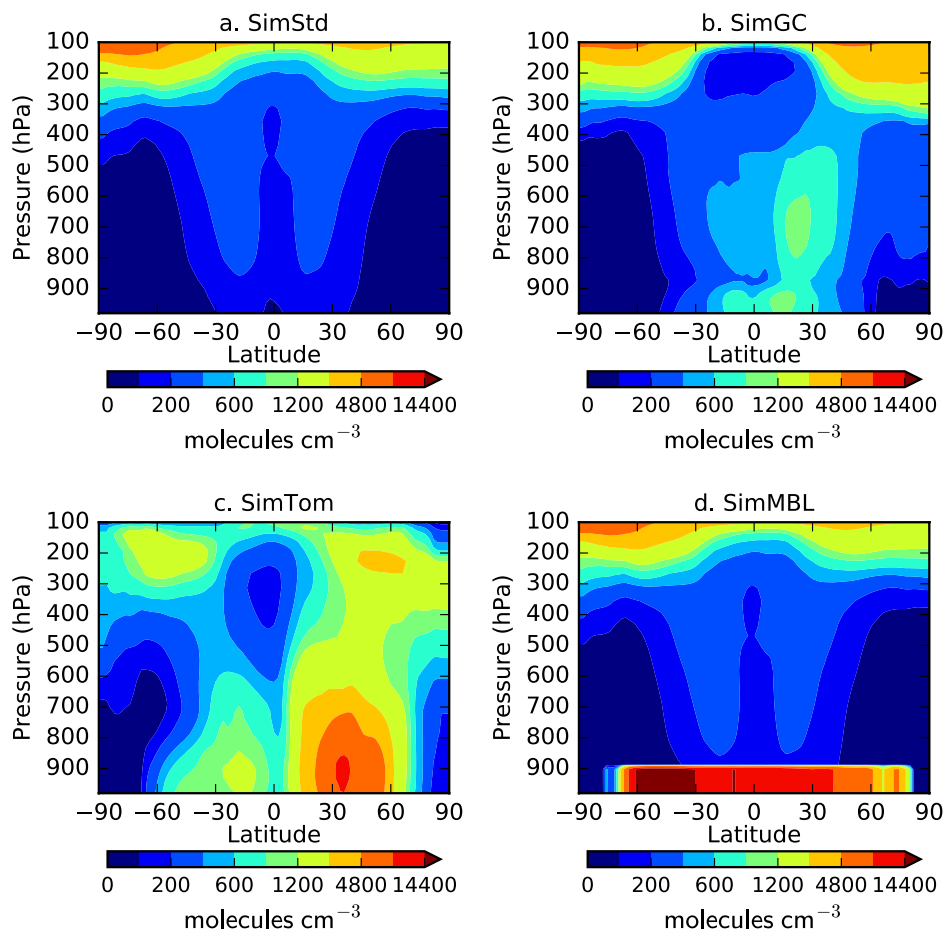
552
553
554
555

Fig. 1: The July 2004 surface concentration of CH₄ (left) and δ¹³C-CH₄ (right) from biomass burning (a,b), wetlands (c,d), and geologic+coal sources (e,f) from the GEOS tagged CH₄ tracers.



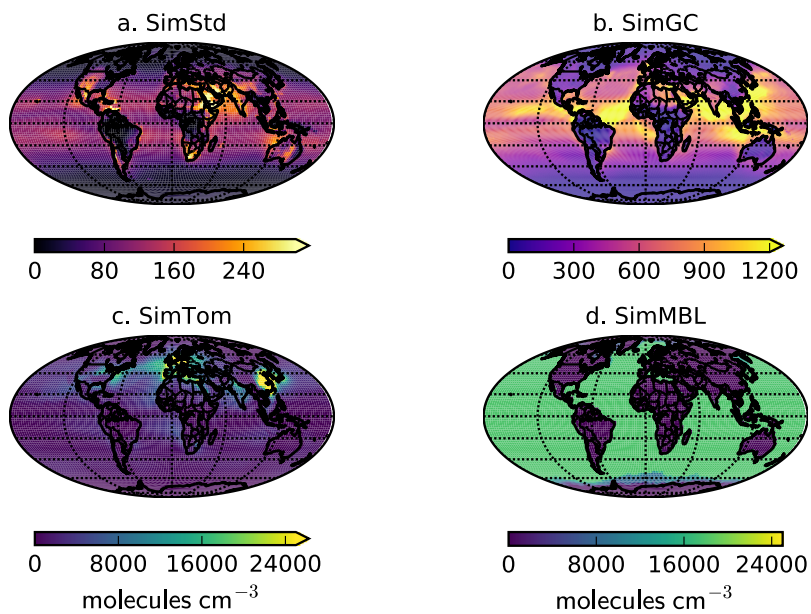
556
557
558
559

Fig 2: Monthly CH₄ observations from the GMD network (black) and simulated surface concentrations from SimStd (red) averaged over latitude bands



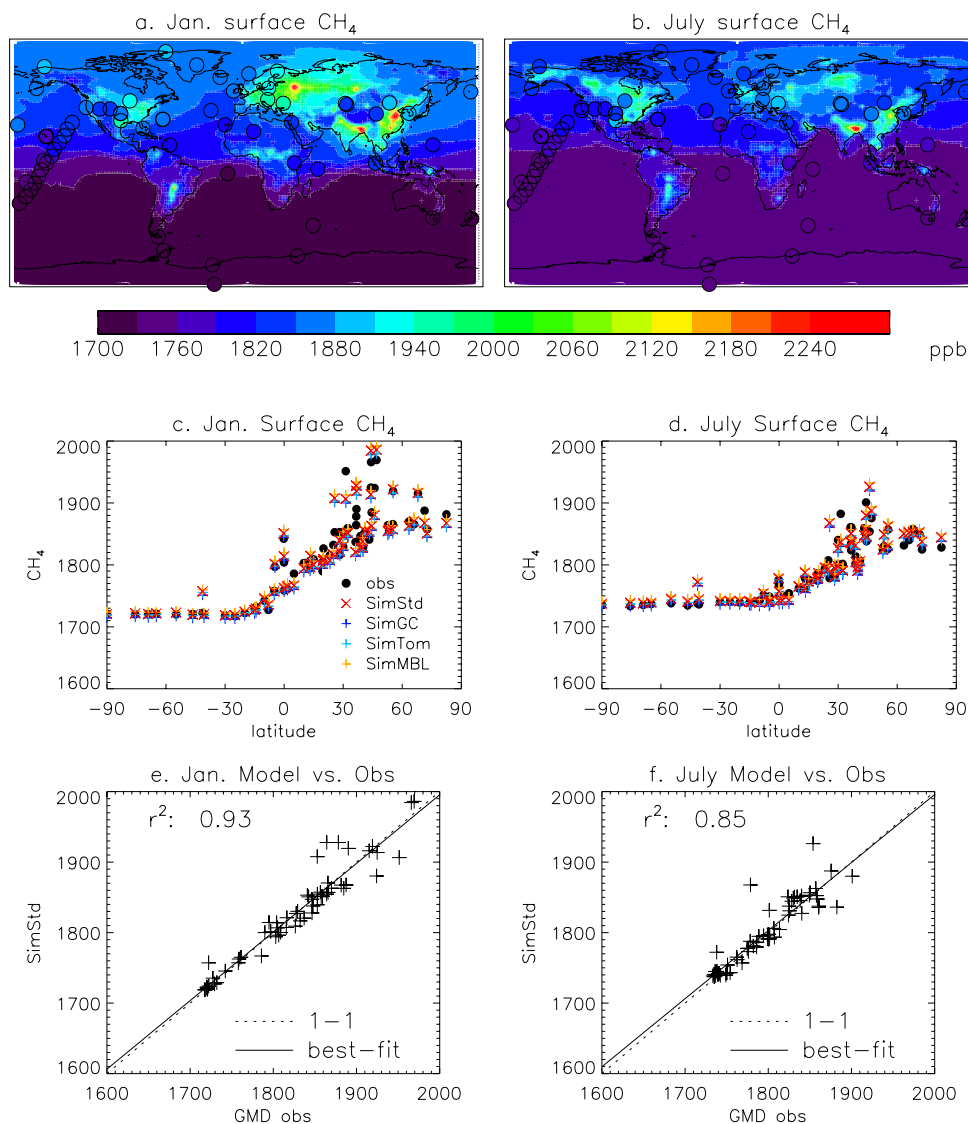
560
561
562

Fig. 3: Annual zonal mean Cl field for a) SimStd, b) SimGC, c) SimTom, and d) SimMBL.

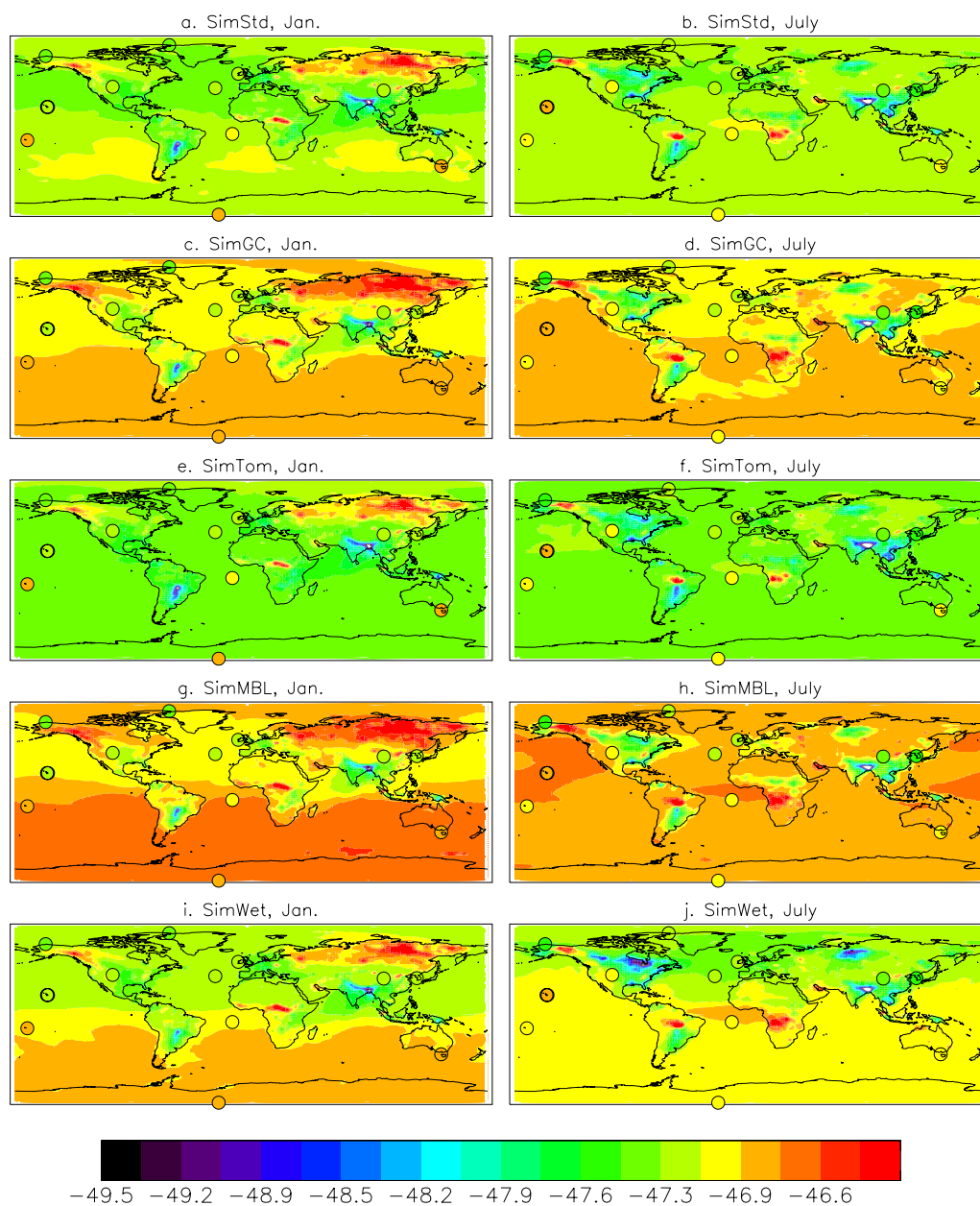


563
564
565
566

Fig. 4: Annual mean surface concentrations of Cl in a) SimStd, b) SimGC, c) SimTom, and d) SimMBL. Note the different color scales between panels.

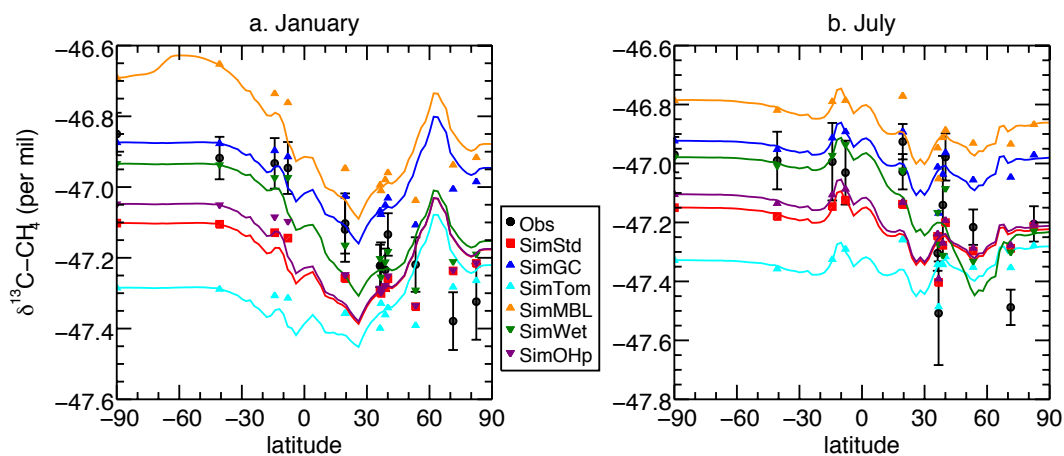


567
 568 **Fig. 5:** Comparison of 2004 simulated and observed surface CH₄ concentrations for January (left) and July (right).
 569 a,b) Surface concentrations of CH₄ from SimStd are overplotted with the concentrations from the GMD observations
 570 in circles. c,d) GMD observations (black circles), SimStd (red x), SimGC (dark blue +), SimTom (light blue +), and
 571 SimMBL (orange +) CH₄ as a function of latitude. E,f) SimStd CH₄ (ppb) at the observation locations versus the
 572 GMD observations (+ signs) as well as the regression line (solid) and 1 to 1 line (dashed).
 573



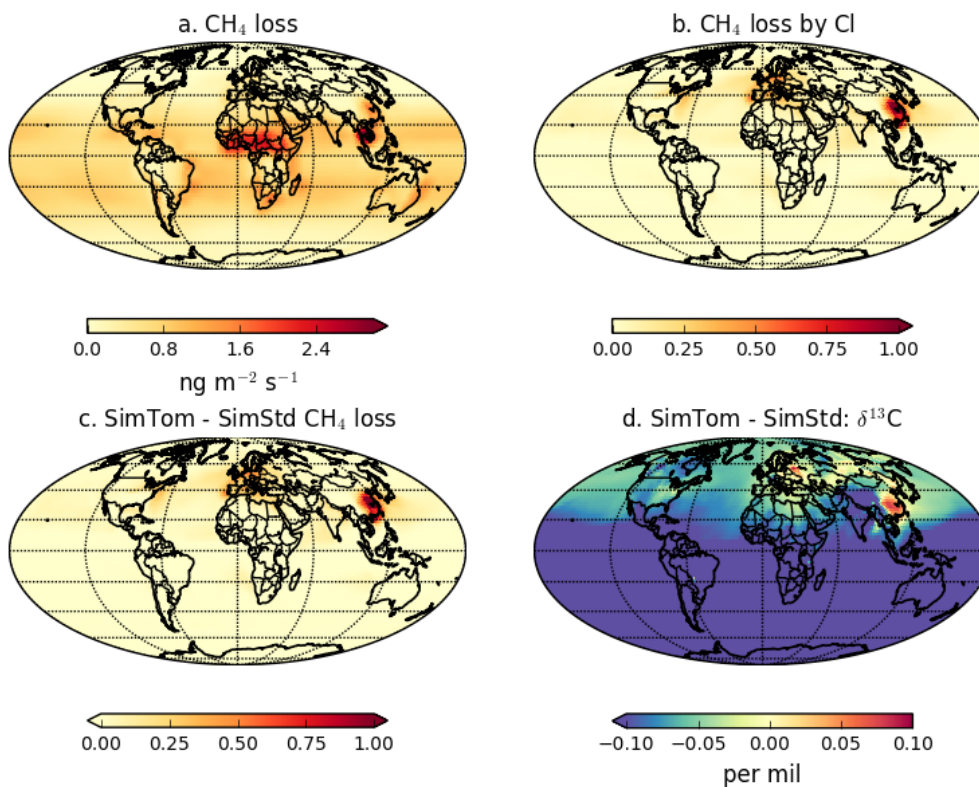
574
575
576
577
578

Fig. 6: Maps of the simulated surface $\delta^{13}\text{C}$ of CH_4 in per mil for Jan. (left) and July (right) overplotted with observations from the GMD sites (circles). The simulations are (a,b) SimStd, (c,d) SimGC, (e,f) SimTom, (g,h) SimMBL, and (i,j) SimWet.



579
 580
 581
 582
 583
 584
 585

Fig. 7: $\delta^{13}\text{C}$ of CH_4 as a function of latitude in a) January and b) July 2004 for the GMD observations (Black circles), SimStd (red), SimGC (dark blue), SimTom (cyan), SimMBL (orange), SimWet (green), and SimOHp (purple). Errorbars represent the maximum of the analytical uncertainty (0.06‰) and the standard deviation of individual measurements in the month for each site. The colored lines represent the simulated zonal mean, while the colored symbols represent the simulation sampled at the location of the GMD observations.

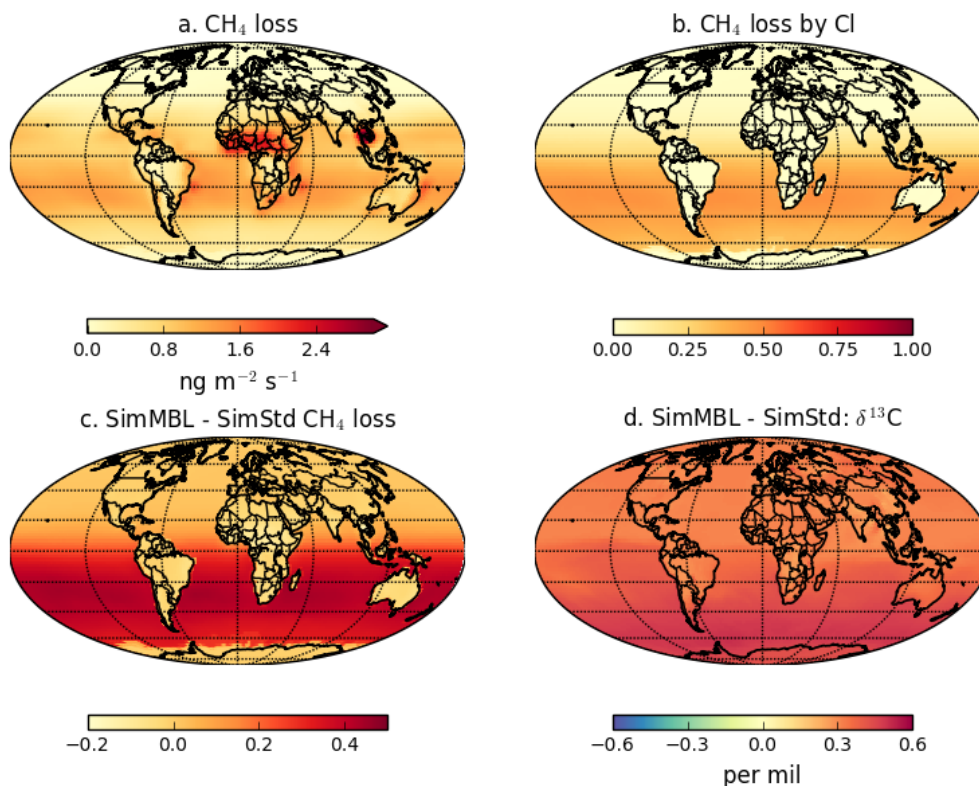


586
 587
 588

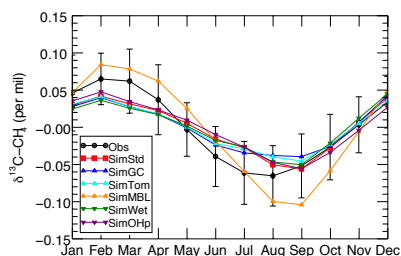
Fig 8: January a) CH_4 loss and b) CH_4 loss by Cl only in the SimTom simulation, as well as the difference in c) CH_4 loss and d) $\delta^{13}\text{C}$ - CH_4 between the SimTom and SimStd simulations.



589



590
591 **Fig 9:** January a) CH₄ loss and b) CH₄ loss by Cl only in the SimMBL simulation, as well as the difference in c)
592 CH₄ loss and d) $\delta^{13}\text{C}$ -CH₄ between the SimMBL and SimStd simulations.
593



594
595 **Fig. 10:** The seasonal cycle of $\delta^{13}\text{C}$ of CH₄ at the SPO site with the annual mean removed averaged over 2002-2004
596 for the GMD observations (black), SimStd (red), SimGC (blue), SimTom (cyan), SimMBL (orange), SimWet
597 (green), and SimOHp (purple). Errorbars represent the standard error, calculated as the maximum of the pooled
598 standard deviation or the analytical uncertainty (0.06%), divided by the square root of the number of years of
599 observations.
600
601